Applied Catalysis B: Environmental 97 (2010) 182–189

Contents lists available at ScienceDirect

Applied Catalysis B: Environmental

journal homepage: www.elsevier.com/locate/apcatb

Effective visible light-active boron and carbon modified TiO_2 photocatalyst for degradation of organic pollutant

Yongmei Wu [a], Mingyang Xing [a], Jinlong Zhang [a,b,*], Feng Chen [a]

[a] Key Laboratory for Advanced Materials and Institute of Fine Chemicals, East China University of Science and Technology, 130 Meilong Road, Shanghai 200237, PR China
[b] School of Chemistry and Materials Science, Guizhou Normal University, Guiyang 550001, PR China

ARTICLE INFO

Article history:
Received 21 December 2009
Received in revised form 28 March 2010
Accepted 29 March 2010
Available online 4 April 2010

Keywords:
C and B modification
Titanium dioxide
Visible light photocatalytic activity
Photocatalyst

ABSTRACT

A visible light-active TiO_2 photocatalyst modified by boron and carbon was synthesized by sol–gel followed solvothermal process. The resulting photocatalyst was characterized by X-ray diffraction (XRD), X-ray photoelectron spectroscopy (XPS), UV–vis absorption spectroscopy, and electron paramagnetic resonance (EPR). It was found that the boron and carbon modified TiO_2 showed obvious absorption in the range 400–500 nm. XPS results suggested boron species entered into interstitial site of TiO_2 matrix and formed the B–O–Ti bond, while carbon species were in the form of carbonates species. EPR results showed the existence of oxygen vacancy in carbon and boron modified TiO_2. This may result in the sensitivity of the as-synthesized photocatalyst to visible light. The resulting boron and carbon modified TiO_2 exhibited significantly higher photocatalytic activity than carbon modified TiO_2 and undoped anatase TiO_2 on the degradation of Acid Orange 7 (AO7) in aqueous solution under visible light irradiation. The presence of carbon originating from organic precursor has great influence on the surface properties of B-doped TiO_2.

1. Introduction

Semiconductor photocatalytic materials have been extensively studied in the fields of environmental purification. In this application, titanium dioxide is most widely used, because it has advantages in inexpensiveness, chemical stability, and nontoxicity in addition to its favorable optoelectronic property [1,2]. However, its wide band gap (3.0–3.2 eV) allows it to absorb only the ultraviolet light which accounts for merely 5% of the solar photons, thereby hampering its wide use. In order to utilize the solar energy efficiently, many studies have been carried out to extend the spectral response of TiO_2 into the visible region and enhance its photocatalytic activity. Recently, a promising way to achieve the visible light activity of TiO_2 is doping TiO_2 with a non-metal element, such as N [3–5], C [6–8], S [9], P [10], and halogen atoms [11]. More recently, boron doping begins to attract attention in electrochemical and functional materials application studies because it is prompting the creation of electron acceptor level [12–21]. However, controversial reports are found in the literature on B-doped TiO_2. On the basis of DFT calculations, Geng et al. [12] reported that boron atoms can be doped into TiO_2 either in the interstitial position or at the O site and the O substitution would lead to narrowing of the bandgap. Contrary to the above mentioned reports, Chen et al. [13] reported that doped boron ion was situated in the interstitial TiO_2 structure, forming a possible chemical environment such as Ti–O–B resulting in blue-shift of the absorption edge of insterstitial B-doped TiO_2 compared to undoped TiO_2. This B-doped TiO_2 photocatalyst showed higher activity than pure TiO_2 sample in the photocatalytic reaction of nicotinamide adenine dinucleotide (NADH) under UV light irradiation. Jung et al. [14] also reported a blue-shift of the light absorption in B-doped TiO_2 when the boron content is less than 5%. On the other hand Yang et al. suggested a red-shift of the absorption edge in substitutional B- to O-doped anatase and blue-shift of absorption in interstitial B-doped anatase [15]. Moon et al. [16] synthesized B-doped TiO_2 using sol–gel method and boric acid triethyl ester as boron source and the B/TiO_2 photocatalyst showed a red-shift in the absorption edge and enhanced photocatalytic activity towards decomposition of water under UV light. Zhao et al. [17] reported that doping TiO_2 with boron and Ni_2O_3 resulted in the improvement of TiO_2 in both visible light response and photocatalytic efficiency. Lambert and co-workers [18] also reported low level of boron doped TiO_2 lead to significant absorption of visible light and better photoactivity for degradation of methyl tert-butyl ether (MTBE) than undoped TiO_2. Zaleska et al. synthesized boron modified TiO_2 using boric acid and boric acid triethyl ester (BATE) by the sol–gel method and by grind-

* Corresponding author at: Lab for Advanced Materials and Institute of Fine Chemicals, East China University of Science and Technology, Shanghai 200237, PR China. Tel.: +86 21 64252062; fax: +86 21 64252062.
E-mail address: jlzhang@ecust.edu.cn (J. Zhang).

0926-3373/$ – see front matter © 2010 Elsevier B.V. All rights reserved.
doi:10.1016/j.apcatb.2010.03.038

ing anatase powder with boron dopant. They acclaimed that boron doping extended absorption edge to visible light region leading to induced activity on the prepared samples on the photooxidation of phenol under visible light instead of under UV light compared to pure TiO_2 [19,20]. The highest photoactivity was observed over the sample obtained by impregnation with 2 wt.% of BATE and calcined at 400 °C. Not only boron species were observed in the B-TiO_2 samples but also carbon species arising from incomplete precursor decomposition were also observed. They proposed that visible light activity of the B-doped sample can be rather related to the presence of boron than carbon. Gombac et al. [21] synthesized B-doped TiO_2 and B–N-codoped TiO_2 photocatalysts by sol–gel followed by calcination process at high temperatures. A blue-shift of absorption edge for B doped TiO_2 was observed with respect to pure anatase and rutile, which was attributed to its lower nanocrystal dimension. Interestingly, even calcination at 450 °C for 6 h, this B-doped photocatalyst containing carbon was confirmed by XPS, which gave a peak located at 286.0 eV related to C–O originating from the organic titanium precursor. It is should be noted that there is some confusion in the assignment of the carbon species in the reported works. It is evident that existence of the carbon in the synthesized TiO_2 is unavoidable due to the organic solvents and the alkoxide groups in the Ti source. As a result, the carbon element is always detected in nearly all the XPS analysis. However, their assignment is rather diverse. In most cases, these C species were ascribed to adventitious carbon which is not responsible for visible response of the photocatalyst [19–21]. Some researchers claimed that these C species could be incorporated into the lattice to replace O and endow the TiO_2 with visible light activity [22–25]. For example, Kisch and co-workers [22] have proved that carbon-containing titania, prepared by a modified sol–gel process using different titanium alkoxide precursors, was able to photodegrade *p*-chlorophenol under visible light ($\lambda > 400$ nm). Colón et al. found the presence of carbon species in TiO_2 samples after calcination at 973 K, which showed a broad spectrum of 400–600 nm, it was proposed that carbon residuals were responsible for the formation of oxygen vacancies in the TiO_2 specimens which could lead to visible light absorption [23]. Yang et al. [24] argued that alkoxide groups of titanium source can also be used as a C source during the sol–gel synthesis of C–N codoped TiO_2. Choi and co-workers reported that carbon-doped TiO_2 prepared from a conventional sol–gel synthesis using titanium alkoxide precursor without adding external carbon precursors and they claimed that the carbons species from titanium alkoxide precursor could be incorporated into the lattice of TiO_2 by a controlled calcination at temperature ranging from 200 to 300 °C [25]. In our previous study, C and N co-doped TiO_2 synthesized by a microemulsion-hydrothemal process without calcinations exhibited better photoactivity for degradation of Rhodamine B under visible light than P25, the carbon species originated from titanium alkoxide could be doped into the lattice of TiO_2 [26]. This shows that the effect of carbon species originating from organic compound on the properties of TiO_2 as well as its photocatalytic performance under visible light cannot be ignored. It was found that B and N codoped TiO_2 [21,27], B and F codoped TiO_2 [28] showed higher photocatalytic activity and peculiar characteristics compared with single element doping into TiO_2. However, to our best knowledge, carbon and boron comodified TiO_2 using sol–gel process followed with solvothermal method under moderate conditions has not yet been reported.

Here we prepared boron and carbon modified TiO_2 by sol–gel followed by solvothermal process. The photoactivity of B and C comodified TiO_2 was evaluated by the photodegradation of Acid orange 7 (AO7) under visible light irradiation. We have found that the presence of carbon species originating from organic precursor has great influence on the surface properties of B-doped TiO_2 as well as its photocatalytic performance.

2. Experimental

2.1. Catalyst preparation

The boron and carbon modified TiO_2 nanoparticles were prepared by combining sol–gel method followed with solvothermal treatment. 6 mL tetrabutyl titanate was dissolved into 17 mL anhydrous ethanol (solution A), solution B consisted of 35 mL anhydrous ethanol, 0.1 mL concentrated nitric acid (68%), 1.6 mL water and the required stoichiometric amount H_3BO_3. Then solution A was added drop-wise to solution B under magnetic stirring. The resultant mixture was stirred at room temperature for 4 h until the transparent sol was obtained. The sol was then aged for two days and the gel was obtained, which was then transferred into a 100 mL Teflon-inner-liner stainless steel autoclave. The autoclave was kept for 10 h under 180 °C for crystallization. After this solvothermal treatment, the precipitate gained was washed by distilled water, dried at 100 °C for 24 h and calcined at 300 °C for 2 h. The boron doping concentration (x) was chosen as 0.5, 1.0, 2.0, 5.0, which was the mole percentage of boron element in the theoretical titania powder. The obtained photocatalysts with corresponding boron concentration were denoted as xB–C–TiO_2. The carbon modified TiO_2 sample was also prepared by the same method in the absence of H_3BO_3, denoted as C–TiO_2. Commercial pure anatase TiO_2 (produced by Shanghai Kangyi Co., Ltd.) with specific surface area of 120 m^2/g and primary particle size of 10 nm were used for comparison purpose. In order to check the effect of carbon, 1.0B–C–TiO_2 was calcined at 300 °C for 2 h under static air, air flow (100 ml/min) and N_2 flow (100 ml/min), respectively and the samples were denoted as 1.0B–C–TiO_2-1, 1.0B–C–TiO_2-2, 1.0B–C–TiO_2-3.

2.2. Catalyst characterization

XRD analysis of the as-prepared photocatalysts was carried out at room temperature with a Rigaku D/max 2550 VB/PC apparatus using Cu Kα radiation ($\lambda = 1.5406$ Å) and a graphite monochromator, operated at 40 kV and 30 mA. Diffraction patterns were recorded in the angular range of 10–80° with a stepwidth of 0.02° s^{-1}. The X-band EPR spectra were recorded at room temperature (Varian E-112). To analyze the light absorption of the photocatalysts, UV–vis absorption spectra were obtained using a scan UV–vis spectrophotometer (Varian Cary 500) equipped with an integrating sphere assembly, while $BaSO_4$ was used as a reference. To investigate the chemical states of the photocatalysts, X-ray photoelectron spectroscopy (XPS) was recorded with PerkinElmer PHI 5000C ESCA System with Al Kα radiation operated at 250 W. The shift of binding energy due to relative surface charging was corrected using the C 1s level at 284.6 eV as an internal standard. The content of carbon in the sample was determined by DTA–TG on a PerkinElmer Pyris Diamond Setaram instrument from room temperature to 800 °C at a constant rate of 10 °C min^{-1} under air with a flow rate of 50 mL min^{-1}.

2.3. Photocatalytic activity test

The photocatalytic activities of samples were evaluated in terms of the degradation of acid orange 7 (AO7) under visible light illumination. The photocatalyst powder (0.08 g) was dispersed in a 100 mL quartz photoreactor containing 80 mL of a 20 mg L^{-1} AO7 solution. The mixture was sonicated for 10 min and stirred for 30 min in the dark in order to reach the adsorption–desorption equilibrium. A 1000 W tungsten halogen lamp equipped with a UV cut-off filters ($\lambda > 420$ nm) was used as a visible light source (the average light intensity was 60 mW cm^{-2}). The lamp was cooled with flowing water in a quartz cylindrical jacket around the lamp, and ambient temperature was maintained during the photocat-

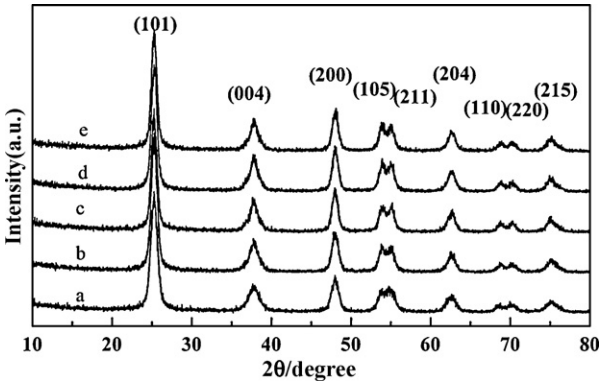

Fig. 1. XRD patterns of samples with different amount of B: (a) C–TiO_2, (b) 0.5B–C–TiO_2, (c) 1.0B–C–TiO_2, (d) 2.0B–C–TiO_2, and (e) 5.0B–C–TiO_2.

alytic reaction. At the given time intervals, the analytical samples were taken from the mixture and immediately centrifuged, then filtered through a 0.22 μm Millipore filter to remove photocatalysts. The concentration of the filtrate was analyzed by checking the absorbance at 484 nm with a UV–vis spectrophotometer (Varian). The reproducibility was checked by repeating the measurements at least three times and was found to be within the acceptable limit (±5%).

•OH radicals generated on the photocatalysts surface under visible light irradiation were investigated using a Varian cary eclipse fluorescence spectrophotometer. About 0.10 g of the photocatalyst was added to 30 ml of terephthalic acid solution with a concentration of 0.83 g/L. The •OH radicals generated by means of visible light irradiation reacted with terephthalic acid to produce high fluorescence hydroxyterephthalic acid. The amount of 2-hydroxyterephthalic acid corresponded to the amount of •OH radicals [29]. The 2-hydroxyterephthalic acid is the only product with any significant fluorescence. The shapes of the spectra characteristic to the reaction product and wavelength of maximum emission were the same, whereas only the intensities of these spectra were changed. To determine the amount of •OH radicals, the peak areas were calculated.

3. Results and discussion

3.1. XRD analysis

XRD was carried out to investigate the changes of C–TiO_2 phase structure after boron doping. Fig. 1 shows the effect of different amount of B dopant on the crystal structure of C–TiO_2 nanoparticles calcined at 300 °C for 2 h. It is found that all diffraction peaks can be perfectly indexed as anatase phase of TiO_2 [JCPDS no. 21-1272, spacegroup: $I4_1/amd$ (1 4 1)]. No significant characteristic peaks for boron oxide were detected. It may be attributed to the lower boron content in these samples beyond the detection limit of XRD technique. According to the line width analysis of the anatase (1 0 1) diffraction peak based on the Scherrer formula, the average crystalline sizes of all these samples estimated by Scherrer formula are summarized in Table 1. As can be seen from Table 1, the crystallite sizes of boron and carbon modified TiO_2 are slightly lower than that of C modified TiO_2, which indicates the occurrence of a slight lattice distortion in the structure of anatase TiO_2.

To further investigate the effect of boron doping on the crystal structure of C–TiO_2, the lattice parameters of all boron doping samples calculated using Bragg's law ($2d \sin\theta = \lambda$) and a formula ($1/d^2 = (h^2 + k^2)/a^2 + l^2/c^2$) for a tetragonal system are listed in Table 1. It is clearly seen that the lattice parameter of *a*-axis for all boron doping samples is unchanged with increase in the amount

Table 1
Lattice parameters of C–TiO_2 with different B doping.

Sample	Crystalline size (nm)	Lattice parameter		C concent wt.%
		a-Axis	*c*-Axis	
C–TiO_2	13.0	3.7856	9.4975	0.8
0.5B–C–TiO_2	12.9	3.7869	9.4992	1.4
1.0B–C–TiO_2	12.7	3.7875	9.5071	1.5
2.0-C–TiO_2	12.4	3.7853	9.5127	0.9
5.0-C–TiO_2	11.0	3.7887	9.4777	1.0

of boron dopant. As amount of boron doping ranges from 0.5% to 2.0%, the lattice parameter of *c*-axis increases, indicating that boron ions may have entered into interstitial site of C–TiO_2 matrix leading to swell of unit cell volume. Considering the radius of B^{3+} (0.023 nm) and Ti^{4+} (0.064 nm), it is difficult for B^{3+} to substitute of Ti^{4+}. DFT calculation for B-doped TiO_2 by some groups showed that B atom can be doped into TiO_2 either in the interstitial position or at the O site [12,15]. The similar experimental phenomenon was also observed by Chen et al. [13]. However, the *c*-axis parameter of 5.0B–C–TiO_2 decreases, which implies that some boron ions may separate from the lattice of TiO_2 and form diboron trioxide, the amount of diboron trioxide is minute, hence below the detection limit of XRD technique.

Fig. 2 shows the effect of calcinations temperature on the phase structure of 5.0B–C–TiO_2. Only anatase phase was observed with the calcination temperatures increasing from 300 to 700 °C, while with respect to C–TiO_2 sample, rutile phase appeared when the calcinations temperature was reached 700 °C (not shown). Our results suggest that doping with B suppressed the phase transformation of anatase to rutile, which is in agreement with literature proposal [13].

3.2. TG–DTA analysis

TG–DTA spectra of uncalcined 1.0B–C–TiO_2 under air atmosphere and under N_2 atmosphere are shown in Fig. 3. It can be seen that the profiles of the two DTA curves at $T < 400$ °C are quite different. 1.0B–C–TiO_2 in air shows a single peak at ca. 280 °C and a shoulder peak at 310 °C. The first one is due to the removal of strongly bound water or surface hydroxyl. The second one can be attributed to decomposition of organic compound. This is an indication that some carbon species exists in the as-prepared sample when calcined at 300 °C under air atmosphere. However, only a broad peak at 150 °C was observed in the sample of 1.0B–C–TiO_2 under nitrogen atmosphere, which is due to the loss of physically

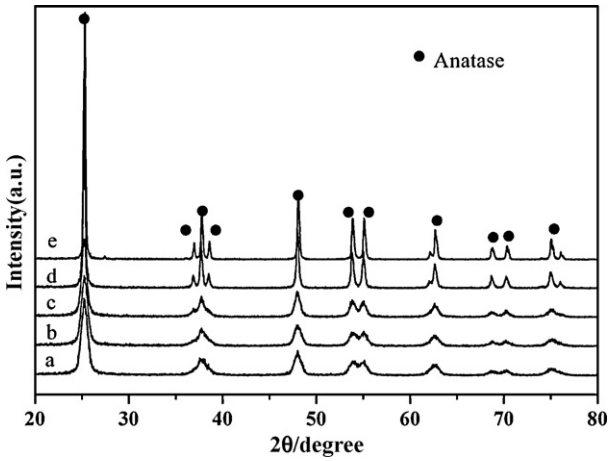

Fig. 2. XRD patterns of 5.0B–C–TiO_2 sample under different calcination temperature: (a) 300, (b) 400, (c) 500, (d) 600, and (e) 700 °C.

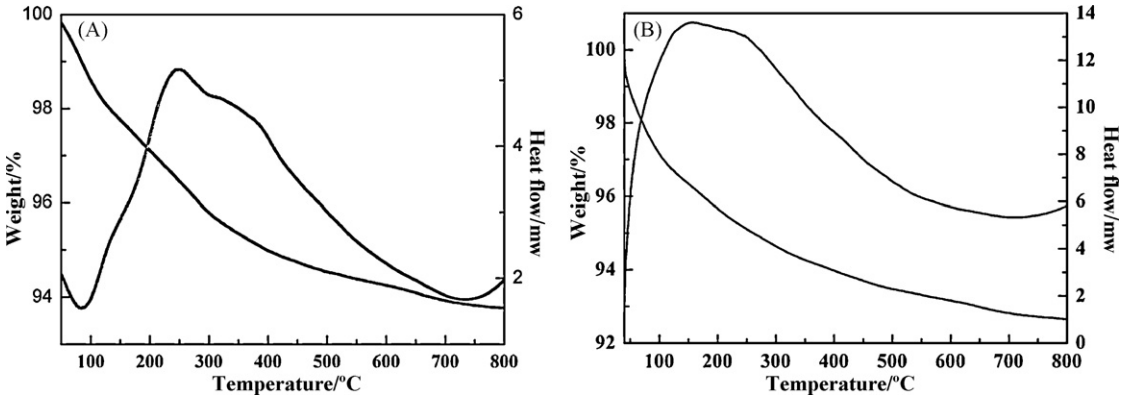

Fig. 3. TG–DTA spectra of uncalcined 1.0B–C–TiO_2 (A) at air atmosphere (B) at N_2 atmosphere.

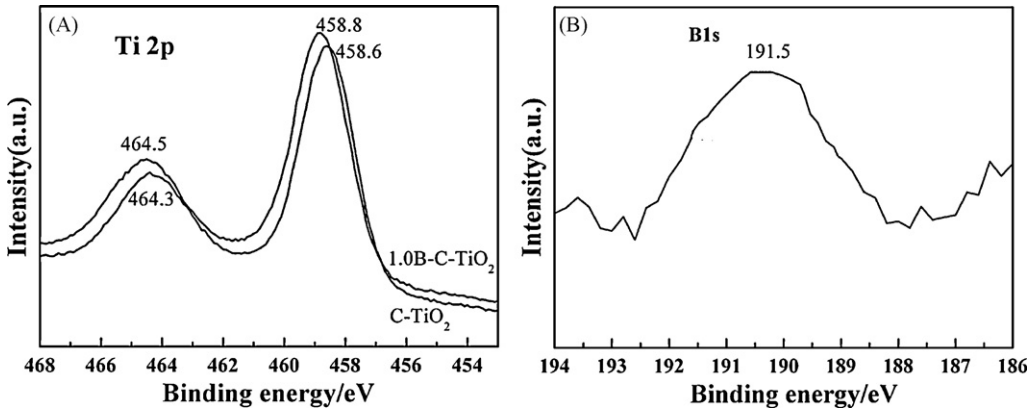

Fig. 4. XPS spectra of C–TiO_2 and 1.0B–C–TiO_2 of (A) Ti 2p (B) B 1s.

adsorbed water. Strongly bound water or surface hydroxyl ions in the sample are slowly being eliminated with the rise of temperature from 100 to 300 °C. Thermogravimetric analysis (TG) is used to estimate the carbon content in the sample. Taking the mass loss of pure TiO_2 as a reference, the carbon content can be calculated to be 1.5, 0.5 and 3.0 wt.% for 1.0B–C–TiO_2-1, 1.0B–C–TiO_2-2 and 1.0B–C–TiO_2-3, respectively. Clearly, the carbon content in the 1.0B–C–TiO_2 samples calcined under nitrogen atmosphere is higher than that of sample with treatment under air atmosphere. Additionally, the C content in the samples with different boron doping are summarized in Table 1. It can be seen that the carbon content in C–TiO_2 sample is about 0.8 wt.%. When the boron doping into TiO_2, the C content in these sample is keep ranging from 0.9 to 1.5 wt.%. Significant variation of carbon content with increasing amount of boron dopant is not observed due to these carbon species coming from organic precursor.

3.3. XPS analysis

Ti 2p XPS spectra of C–TiO_2 and 1.0B–C–TiO_2 samples are shown in Fig. 4(A) The binding energies of Ti $2p_{3/2}$ and Ti $2p_{1/2}$ for C–TiO_2 sample is at 458.6 and 464.3 eV, which agree with Ti(IV) in titanium oxide [30]. Compared to C–TiO_2 sample, Ti 2p peaks show positive shift of 0.2 eV for 1.0B–C–TiO_2 sample. It was reported that boron doping favor the formation of Ti^{3+} on the surface or subsurface layer of TiO_2 [31]. But in our XPS result there is no evidence of Ti^{3+} formation. This may be attributed to low amounts of Ti^{3+} which could not be detected by XPS technique. For 1.0B–C–TiO_2 sample, the B 1s appears at the binding energy of 191.5 eV (Fig. 4(B)). Based on XPS results, the B concentrations were 0.72% (atom ration). Peaks at 187.5 eV corresponding to B–Ti bond in TiB_2 and peak at 193.0 eV corresponding B-O from B_2O_3 were not found in our sample. As reported by Lambert and co-workers [18], low binding energy peak at 190.6 eV corresponds to species capable of inducing the unprecedented visible light photocatalytic activity of B-doped TiO_2. However, this peak did not appear in the B 1s spectra either. Chen et al. [13] and Huo et al. [32] suggested that the peak at 191.5 eV may be assigned to B atom in the interstitial position of TiO_2 and formation of B–O–Ti bond. Therefore, we assume that the peak at 191.5 eV corresponds to B atoms in the interstitial position of TiO_2 and formation of B–O–Ti bond.

C1s XPS spectra of C–TiO_2, 1.0B–C–TiO_2-1 and 1.0B–C–TiO_2-3 samples are shown in Fig. 5. There are two XPS peaks at 284.6 and 288.3–288.5 eV observed among these samples which could be the contribution of two states of carbon species. The lower binding energy at 284.6 eV is associated with the adventitious elemental carbon [33,34]. Another peak at 288.5 eV suggests the existence of C–O, indicating the formation of carbonated species [6,23]. Kisch and co-worker suggested that this peak should be related to the carbonate species as an interstitial dopant [6,23]. Ren et al. [35] and Li et al. [8] proposed that carbon may substitute some of the lattice titanium atoms and form a Ti–O–C structure. The origin of visible light absorption of carbon modified TiO_2 is mostly ascribed to interstitial carbon doping. We agree with Kisch's opinion, this peak can be an interstitial doping carbon species. Some reports have also confirmed that carbon species originating from the organic titanium precursor could be doped into the TiO_2 [22,24,25].

3.4. UV–vis absorption spectra

Fig. 6(A) shows the UV–vis absorption spectra of C–TiO_2 and C–B–TiO_2 samples compared with commercial pure anatase TiO_2.

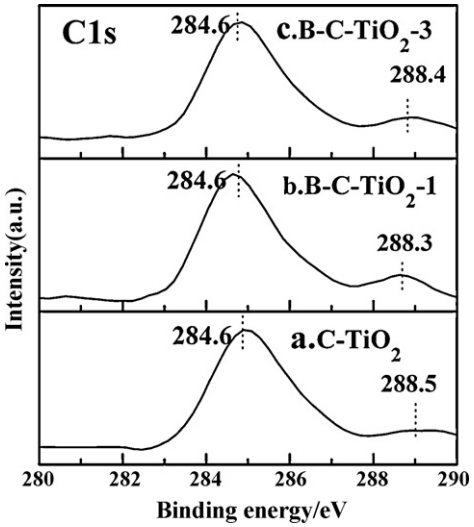

Fig. 5. C1s XPS spectra of C–TiO_2 and 1.0B–C–TiO_2 sample calcined in static air and N_2 flow

The band gap energies were determined from a plot $(\alpha h\nu)^{1/2}$ versus photon energy($h\nu$) using the following equation which shows indirect relationship of the absorption coefficient α and band gap E_g. [36]

$$(\alpha h\nu)^{1/2} \infty h\nu - E_g$$

where ν is the frequency and h is Planck's constant. The Tauc plot, $(\alpha h\nu)^{1/2}$ versus $h\nu$, is shown in Fig. 6(B). The pure anatase TiO_2 has the band gap energy of 3.08 eV. The band gap for C–TiO_2 sample is about 2.92 eV, which is smaller than that of pure anatase TiO_2. In the case of 1.0B–C–TiO_2 and 5.0B–C–TiO_2, they have the same band gap energy of 2.85 eV indicating that low level of B doping has no significant influence on E_g probably due to the formation new phase of B_2O_3. Similar results have been obtained by Huo et al. [32]. The origin of absorption bands in the visible spectral range for anion doped TiO_2 specimens remains a hot topic of discussion. Some researchers reported that anion modification in titania increases visible light absorption by introducing localized states in the band gap [9,37], while some of studies revealed that intrinsic defects, including those defects associated with oxygen vacancies, contribute to the absorption of light in the visible spectral region [38,39]. A recent study by Kuznetsov and Serpone has proposed that the commonality in all these anion doped titania rests with formation of oxygen vacancies and the advent of color centers that absorb the visible light radiation [40]. Ke and co-workers [41] have proposed that boron doping favors formation of an oxygen vacancy with two excess electrons, which would further reduce two Ti^{4+} ions to form Ti^{3+}. So we assume that B doping may lead to increased formation of oxygen vacancies and thus slightly improving the visible photoabsorption capability.

Fig. 7(A) and (B) shows the UV–vis absorption spectra of 1.0B–C–TiO_2 at calcinations under different gas atmosphere. It can be seen that the band gap energy of 1.0B–C–TiO_2 under air flow, static air and nitrogen flow are 2.95, 2.85 and 2.73 eV, respectively. Obviously, the decrease of band gap energy is related to the carbon content. Kisch et al. also reported that the optical properties of carbon modified TiO_2 are related to carbon content [6].

3.5. EPR spectra analysis

EPR spectra of C–TiO_2 and 1.0B–C–TiO_2 samples calcined in static air and N_2 flow recorded at ambient temperature are shown in Fig. 8. The symmetric signal at $g = 2.004$ was detected in C–TiO_2 and 1.0B–C–TiO_2 samples calcined in static air and N_2 flow. Nakamura et al. [42] reported that the symmetrical and sharp EPR signal at $g = 2.004$ detected on plasma-treated TiO_2 arose from the electron trapped on the oxygen vacancy. Serwicka [43] observed a sharp signal at $g = 2.003$ on the vacuum-reduced TiO_2 at 673–773 K. They attributed this signal to a bulk defect, probably an electron trapped on an oxygen vacancy. Similar EPR signal has been observed in C-doped anatase TiO_2 [8,21,44] and B-doped TiO_2 [31]. Li et al. [8] also reported that the used carbon-doped titania still had a strong EPR signal at $g = 2.0055$ after use in photocatalytic test. Interestingly, similar signal ($g = 2.004$) was also found in N-doped TiO_2 by Feng et al. [45]. Serpone and co-workers assigned the signal at $g = 2.003$–2.005 to the one electron trapped on the oxygen vacancy or referred to as an *F* center vacancy [40]. It was reported that the *F* center vacancy located below the band conduction edge of TiO_2 results in the reduced TiO_x and anion doped TiO_2 photocatalyst to be responsive to visible light [40]. It can be seen that the intensity of this signal for 1.0B–C–TiO_2 sample became stronger after introducing boron species. This result suggests that B doping favors the formation of oxygen vacancy. Compared to 1.0B–C–TiO_2 sample calcined in static air, 1.0B–C–TiO_2 samples calcined in N_2 flow shows stronger intensity, implying that much more *F* center vacancy are produced and this is related to the content of carbon. Feng et al. also observed the visible light photoactivity increase in N doped TiO_2 with the intensity of the major peak at $g = 2.004$ from which it was deduced that the *F* defects were formed in a well crystallized TiO_2 surface layer [45]. Another broad signal of $g = 2.146$ for 1.0B–C–TiO_2 samples calcined in N_2 flow may be attributed to photo-generated hole trapped species [44]. So it is reasonable to assume that *F* center vacancy actually exist in the C–TiO_2 and B, C modified TiO_2 and the existence of oxygen vacancy results in the sensitivity of the as-synthesized photocatalyst to visible light.

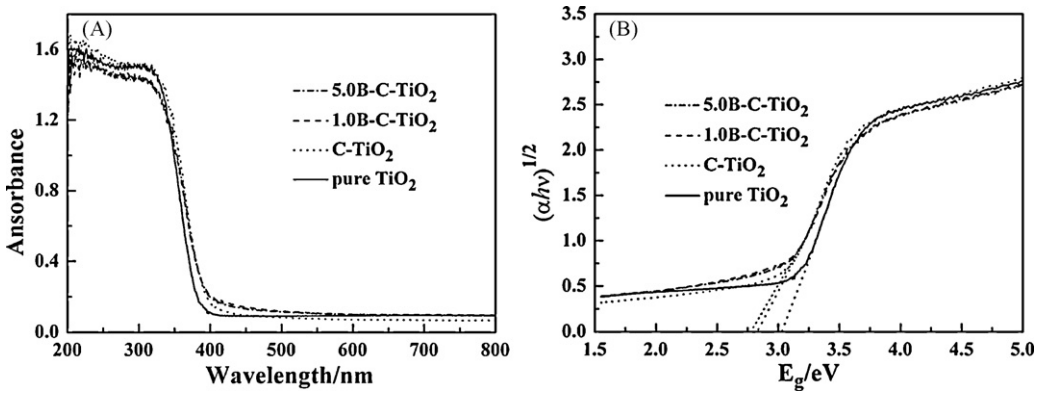

Fig. 6. (A) Diffuse reflectance spectra of C–TiO_2 with different B doping and (B) plot of transformed Kubelka–Munk function versus the energy of the light absorbed.

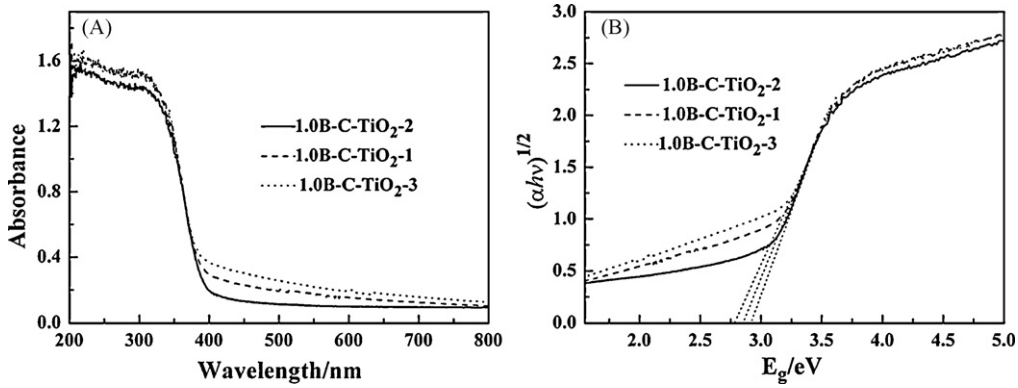

Fig. 7. (A) Diffuse reflectance spectra of C–TiO_2 calcined under different gas atmosphere and (B) plot of transformed Kubelka–Munk function versus the energy of the light absorbed.

Additionally, the content of carbon has an important role in the formation of *F* center vacancy as well as photocatalytic activity.

3.6. Photocatalytic activity

Fig. 9 shows the dependence of photocatalytic degradation of AO7 under visible light irradiation on pure anatase TiO_2, C–TiO_2 and B and C modified TiO_2. The degradation rate of AO7 on the pure anatase TiO_2 under visible light irradiation is very low, which can be attributed to the self-sensitization of AO7. Obviously, the photocatalytic activity of C–TiO_2 is superior to that of pure TiO_2 for the degradation of AO7. Besides the self-sensitization of AO7, the carbonate species on the surface of C–TiO_2 cause the absorption edge extension to visible light range and thus play an important role in improving visible light photoactivity. When a small amount of B atoms were introduced into C–TiO_2 powders, the visible light-induced photocatalytic activities of the prepared samples were enhanced. At 1.0% B dopant, the photocatalytic activity of B and C modified TiO_2 sample reached a maximum value, and its activity exceeded that of pure anatase TiO_2 by a factor of more than three. With further increase of the amount of B dopant, the photocatalytic activity of the sample decreased, indicating that excess amount of boron would become the recombination centers of the photoinduced electrons and holes, which is detrimental to photocatalytic reactions.

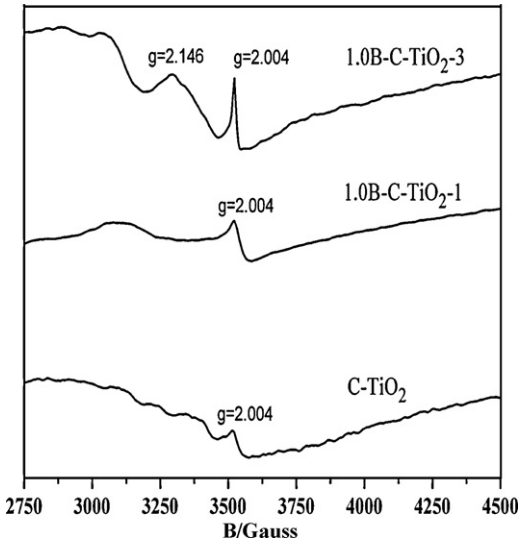

Fig. 8. EPR spectra of C–TiO_2 and 1.0B–C–TiO_2 samples calcined in static air and N_2 flow.

The higher photocatalytic activity of boron and carbon modified TiO_2 here observed may be attributed to the following reasons. On the one hand, both boron and carbon modifications lead to a narrower band gap than C–TiO_2, as discussed previously, which benefits the generation of more photo-induced electrons and holes to participate in the reaction. On the other hand, B doping compared to C doping could improve the amount of oxygen vacancies which is confirmed by EPR result. The existence of these oxygen vacancies in the photocatalyst would act as electron trapping centers, which would avoid the recombination process leaving holes free to proceed to the surface and participate in the photocatalytic process by a mechanism involving direct or indirect oxidation by holes, leading to the enhanced quantum efficiency [46,47]. Gombac and co-workers suggested that B-doping creates reduced Ti^{3+} centers and fivefold coordinated Ti^{3+} ions associated with the presence of oxygen vacancies at the surface were able to reduce molecular oxygen to reactive superoxide species [31]. According to Di Valentin's DFT calculation, they proposed that boron in interstitial positions could behave as a three-electron donor with formation of B^{3+} and reduction of Ti^{4+} to Ti^{3+}, which favors the formation of oxygen vacancies [48]. Our experimental result demonstrated that B doping favors the formation of amount of oxygen vacancies that facilitate the separation and transfer of charge carriers, thereby promoting the photocatalytic activity. Therefore, the synergic contributions from the enhanced absorption in the visible light region and the improved quantum efficiency result in the enhanced vis-photocatalytic activities for boron and carbon modified TiO_2 photocatalysts.

Fig. 10 shows the dependence of photocatalytic degradation of AO7 under visible light irradiation on 1.0B–C–TiO_2 calcined

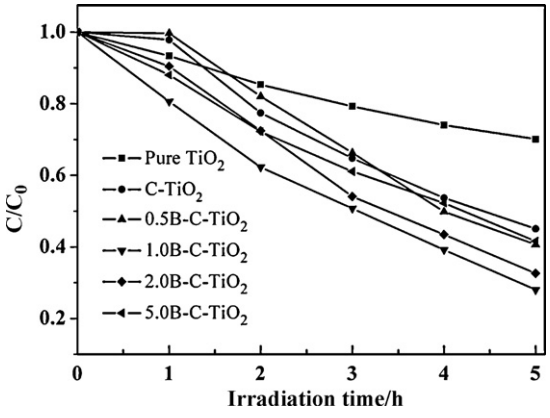

Fig. 9. AO7 degradation under visible light illumination for 5 h in the presence of C–TiO_2 with different boron doping, pure anatase TiO_2.

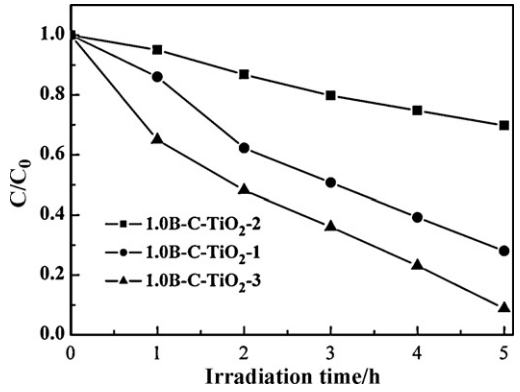

Fig. 10. AO7 degradation under visible light illumination for 5 h in the presence of 1.0B–C–TiO_2 calcined under different gas atmosphere.

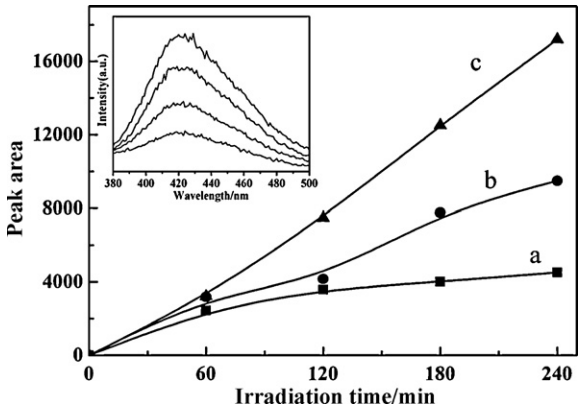

Fig. 11. Plots of the induced fluorescence peak area at 426 nm against irradiation time for terephthalic acid on 1.0B–C–TiO_2 calcined under different gas atmosphere (a) 1.0B–C–TiO_2-2, (b) 1.0B–C–TiO_2-1, (c) 1.0B–C–TiO_2-3.

under different gas atmosphere. 1.0B–C–TiO_2 calcined under N_2 flow exhibits the highest photoactivity among these samples, indicating that higher concentration of carbon would produce both visible light absorption and high photocatalytic efficiency. It was suggested that carbon modification would affect the surface property of TiO_2 such as •OH generation under UV or visible light irradiation [49]. The analysis of •OH radical's formation on the surface of sample under visible light irradiation was performed by fluorescence technique using terephthalic acid, which readily reacted with •OH radicals to produce highly fluorescent product, 2-hydroxyterephthalic acid. The intensity of the peak attributed to 2-hydroxyterephtalic acid is proportional to the amount of •OH radicals formed [50].

In Fig. 11 the formation of •OH radicals on the surface of 1.0B–C–TiO_2 under calcinations under different gas atmosphere is shown with time of visible light irradiation. The amount of the produced •OH radicals increases with visible irradiation time. It can be seen that 1.0B–C–TiO_2 calcined under air flow produce less amount of •OH radicals than 1.0B–C–TiO_2 calcined under N_2 flow and static air. Meanwhile, the highest amount of OH radicals was created in the 1.0B–C–TiO_2 calcined under N_2 flow, which showed the highest photoactivity amongst these three kinds of photocatalysts. It was reported that •OH radicals play important roles in the liquid phase of photodegradation of organic pollutants [51]. Generally, the presence of surface oxygen deficiencies can act as capture centers for the photoexcited electrons, and then transfer the electrons to adsorbed molecular oxygen to produce superoxide O_2^-. This superoxide O_2^- radicals react with proton forming H_2O_2, which can produce free •OH radicals [51]. Our EPR result shows that more oxygen vacancies are produced in the 1.0B–C–TiO_2 calcined under N_2 flow hence can serve as color centers (*F* vacancy center) and make it more active under visible light. Therefore these oxygen vacancies are not only beneficial for the production of more free •OH radicals, but also effectively restrain the recombination of electrons and holes, thus enhancing the photoactivities. Some reports on carbon modified TiO_2 have confirmed that carbon doping could improve the ability for •OH radicals generation [49,52]. Therefore, it is reasonable to conclude that the presence of carbon originating from organic precursor has great influence on the surface properties of TiO_2.

4. Conclusions

The boron and carbon modified TiO_2 was prepared by sol–gel followed solvothermal process. The doping of boron could efficiently inhibit the grain growth and suppress the anatase to rutile transformation. The presence of boron and carbon favors the formation of oxygen vacancies and the advent of color centers that absorb the visible light radiation. All boron and carbon modified TiO_2 showed increased photoactivity over that pure anatase TiO_2 and carbon modified TiO_2 in the photodegradation of AO7 under visible light illumination. This is due to more oxygen vacancies induced by B and C modification which could capture photo-induced electrons and thus inhibit their recombination with photo-induced holes, leading to the enhanced quantum efficiency. Moreover, boron and carbon modified TiO_2 calcined under N_2 atmosphere exhibited higher photoactivity owning to good visible absorption ability and highest amount of •OH radicals created. Therefore, the presence of carbon originating from organic precursor has great influence on the surface properties of B and C modified TiO_2.

Acknowledgments

This work has been supported by National Nature Science Foundation of China (20773039, 20977030), National Basic Research Program of China (973 Program, 2007CB613301, 2010CB732306) and the Ministry of Science and Technology of China (2006AA06Z379, 2006DFA52710).

References

[1] A. Fujishima, T.N. Rao, D.A. Tryk, J. Photochem. Photobiol. C 1 (2000) 1–21.
[2] M.R. Hoffmann, S.T. Martin, W. Choi, D.W. Bahnemann, Chem. Rev. 95 (1995) 69–96.
[3] R. Asashi, T. Morikawa, T. Ohwakl, K. Aoki, Y. Taga, Science 293 (2001) 269–271.
[4] C. Burda, Y. Lou, X. Chen, A.C. Samia, J. Stout, J.L. Gole, Nano Lett. 3 (2003) 1049–1051.
[5] Y. Cong, J.L. Zhang, F. Chen, M. Anpo, D. He, J. Phys. Chem. C 111 (2007) 10618–10623.
[6] S. Sakthivel, H. Kisch, Angew. Chem. Int. Ed. 42 (2003) 4908–4911.
[7] C. Xu, R. Killmeyer, M.L. Gray, S.U.M. Khan, Appl. Catal. B: Environ. 64 (2006) 312–317.
[8] Y. Li, D.S. Hwang, N.H. Lee, S.J. Kim, Chem. Phys. Lett. 404 (2005) 25–29.
[9] H. Luo, T. Takata, Y. Lee, J. Zhao, K. Domen, Y. Yan, Chem. Mater. 16 (2004) 846–849.
[10] L. Lin, W. Lin, J.L. Xie, Y.X. Zhu, B.Y. Zhao, Y.C. Xie, Appl. Catal. B: Environ. 75 (2007) 52–58.
[11] D. Li, H. Haneda, S. Hishita, N. Ohashi, Chem. Mater. 17 (2005) 2588–2595.
[12] H. Geng, S. Yin, X. Yang, Z. Shuai, B. Liu, J. Phys.: Condens. Mater. 18 (2006) 87–96.
[13] D. Chen, D. Yang, Q. Wang, Z. Jiang, Ind. Eng. Chem. Res. 45 (2006) 4110–4116.
[14] Y. Jung, S.B. Park, S.K. Ihm, Appl. Catal. B: Environ. 51 (2004) 239–245.
[15] K. Yang, Y. Dai, B. Huang, Phys. Rev. B 195 (2007) 109201–109206.
[16] S.C. Moon, H. Mametsuka, S. Tabata, E. Suzuki, Catal. Today 58 (2000) 125–132.
[17] W. Zhao, W. Ma, C. Chen, J. Zhao, Z. Shuai, J. Am. Chem. Soc. 126 (2004) 4782–4783.
[18] S. In, A. Orlov, R. Berg, F. García, S.P. Jimenez, M.S. Tikhov, D.S. Wright, R.M. Lambert, J. Am. Chem. Soc. 129 (2007) 13790–13791.
[19] A. Zaleska, J.W. Sobczak, E. Grabowska, J. Hupka, Appl. Catal. B: Environ. 78 (2008) 92–100.
[20] A. Zaleska, E. Grabowska, J.W. Sobczak, M. Gazda, J. Hupka, Appl. Catal. B: Environ. 89 (2009) 469–475.

[21] V. Gombac, L.D. Rogatis, A. Gasparotto, G. Vicario, T. Montini, D. Barreca, G. Balducci, P. Fornasiero, E. Tondello, M. Graziani, Chem. Phys. 339 (2007) 111–123.
[22] C. Lettmann, K. Hildenbrand, H. Kisch, W. Macyk, W.F. Maier, Appl. Catal. B: Environ. 32 (2001) 215–227.
[23] G. Colón, M.C. Hidalgo, G. Munuera, I. Ferino, M.G. Cutrufello, J.A. Navío, Appl. Catal. B: Environ. 63 (2006) 45–59.
[24] X. Yang, C. Cao, L. Erickson, K. Hohn, R. Maghirang, K. Klabunde, J. Catal. 260 (2008) 128–133.
[25] Y. Park, W. Kim, H. Park, T. Tachikawa, T. Majima, W. Choi, Appl. Catal. B: Environ. 91 (2009) 355–361.
[26] Y. Cong, F. Chen, J.L. Zhang, M. Anpo, Chem. Lett. 35 (2006) 800–801.
[27] G. Liu, Y.N. Zhao, C.H. Sun, F. Li, G.Q. Lu, H.M. Cheng, Angew. Chem. Int. Ed. 47 (2008) 4516–4520.
[28] E.A. Reyes-Garcia, Y. Sun, D. Raftery, J. Phys. Chem. C 111 (2007) 17146.
[29] K. Ishibashi, A. Fujishima, T. Watanabe, K. Hashimoto, J. Photochem. Photobiol. A: Chem. 134 (2000) 139–142.
[30] J.F. Zhu, F. Chen, J.L. Zhang, H.J. Chen, M. Anpo, J. Mol. Catal. A: Chem. 216 (2004) 35–43.
[31] M. Fittipaldi, V. Gombac, T. Montini, P. Fornasiero, M. Graziani, Inorg. Chim. Acta 361 (2008) 3980–3987.
[32] Y. Huo, X. Zhang, Y. Jin, J. Zhu, H. Li, Appl. Catal. B: Environ. 83 (2008) 78–84.
[33] S.Y. Treschev, P.W. Chou, Y.H. Tseng, J.B. Wang, E.V. Perevedentseva, C.L. Cheng, Appl. Catal. B: Environ. 79 (2008) 8–16.
[34] E. Papirer, R. Lacroix, J.B. Donnet, G. Nanse, P. Fioux, Carbon 33 (1995) 63–72.
[35] W. Ren, Z. Ai, F. Jia, L. Zhang, X. Fan, Z. Zou, Appl. Catal. B: Environ. 69 (2007) 138–144.
[36] J. Tauc, Mater. Res. Bull. 5 (1970) 721–729.
[37] X. Chen, C. Burda, J. Am. Chem. Soc. 130 (2008) 5018–5019.
[38] V.N. Kuznetsov, N. Serpone, J. Phys. Chem. B 110 (2006) 25203–25209.
[39] N. Serpone, J. Phys. Chem. B 110 (2006) 24287–24293.
[40] V.N. Kuznetsov, N. Serpone, J. Phys. Chem. C 113 (2009) 15110–15123.
[41] N.O. Gopal, H.H. Lo, S.C. Ke, J. Am. Chem. Soc. 130 (2008) 2760–2761.
[42] I. Nakamura, N. Negishi, S. Kutsuna, T. Ihara, S. Sugihara, K. Takeuchi, J. Mol. Catal. A: Chem. 161 (2000) 205–212.
[43] E. Serwicka, Colloids Surf. 13 (1985) 287–293.
[44] E.A.R. Garcia, Y. Sun, K.R.R. Gil, D. Raftery, Solid State Nucl. Mag. Reson. 35 (2009) 74–81.
[45] C. Feng, Y. Wang, Z. Jin, J. Zhang, S. Zhang, Z. Wu, Z. Zhang, New J. Chem. 32 (2008) 1038–1046.
[46] Z. Lin, A. Orlov, R.M. Lambert, M.C. Payne, J. Phys. Chem. B 109 (2005) 20948–20952.
[47] C. Di Valentin, G. Pacchioni, A. Selloni, Phys. Rev. Lett. 97 (2006) 166803–166804.
[48] E. Finazzi, C. Di Valentin, G. Pacchioni, J. Phys. Chem. C 113 (2009) 220–228.
[49] M. Janus, E. Kusiak, A.W. Morawski, Catal. Lett. 131 (2009) 506–511.
[50] T. Hirakawa, Y. Nosaka, Langmuir 18 (2002) 3247–3254.
[51] A. Fujishima, X. Zhang, D.A. Tyrk, Surf. Sci. Rep. 63 (2008) 515–582.
[52] Q. Xiao, L. Ouyang, Chem. Eng. J. 148 (2009) 248–253.